scientific reports

Check for updates

OPEN

The Hippo pathway regulates density-dependent proliferation of iPSC-derived cardiac myocytes

Abigail C. Neininger[1,2], Xiaozhaun Dai[3], Qi Liu[3] & Dylan T. Burnette[1,2]✉

Inducing cardiac myocytes to proliferate is considered a potential therapy to target heart disease, however, modulating cardiac myocyte proliferation has proven to be a technical challenge. The Hippo pathway is a kinase signaling cascade that regulates cell proliferation during the growth of the heart. Inhibition of the Hippo pathway increases the activation of the transcription factors YAP/TAZ, which translocate to the nucleus and upregulate transcription of pro-proliferative genes. The Hippo pathway regulates the proliferation of cancer cells, pluripotent stem cells, and epithelial cells through a cell–cell contact-dependent manner, however, it is unclear if cell density-dependent cell proliferation is a consistent feature in cardiac myocytes. Here, we used cultured human iPSC-derived cardiac myocytes (hiCMs) as a model system to investigate this concept. hiCMs have a comparable transcriptome to the immature cardiac myocytes that proliferate during heart development in vivo. Our data indicate that a dense syncytium of hiCMs can regain cell cycle activity and YAP expression and activity when plated sparsely or when density is reduced through wounding. We found that combining two small molecules, XMU-MP-1 and S1P, increased YAP activity and further enhanced proliferation of low-density hiCMs. Importantly, these compounds had no effect on hiCMs within a dense syncytium. These data add to a growing body of literature that link Hippo pathway regulation with cardiac myocyte proliferation and demonstrate that regulation is restricted to cells with reduced contact inhibition.

Cardiac myocytes (CMs) are the cells of the heart that generate contractile force. The mechanisms controlling CM proliferation are critical during both heart development and disease[1,2]. While adult CMs are non-mitotic, CMs in the developing heart proliferate to drive hyperplastic growth[3–5]. The Hippo pathway has been shown to regulate proliferation during development[6,7]. The Hippo pathway is a kinase cascade that, when active, negatively regulates the transcriptional coactivators YAP and TAZ. In the absence of inhibition, YAP and TAZ translocate to the nucleus to activate the transcription of pro-proliferative genes[8–10]. In addition, the Hippo pathway regulates contact-dependent cell proliferation in epithelial cells, cancer cells, and pluripotent stem cells[11–14]. In these studies, low density cells with fewer cell–cell contacts have increased YAP nuclear localization, while high density cells have more inactive YAP in the cytosol[15,16]. This evidence supports the notion that cell proliferation is not entirely regulated by paracrine mechanisms (e.g., by growth factors) and that proliferation is in part regulated spatially by density-dependent mechanisms[17]. We asked if the Hippo pathway is involved in non-paracrine mechanisms such as contact inhibition in the heart.

The Hippo pathway is required for cardiac development in mice[18,19]. Cardiac-specific knockout of YAP is lethal in mice and leads to thin ventricular walls and several other structural abnormalities[7]. A YAP mutant that blocks the interaction between YAP and its binding partner, the transcription factor TEAD, also led to less proliferation in the developing mouse heart[18]. In addition, during the first post-natal week, the mouse heart retains the ability to fully regenerate after an infarction. YAP conditional knockout mice lose the ability to regenerate[7]. Interestingly, constitutively active YAP can induce CM proliferation in the adult mouse heart, as can a mouse with a conditional knockout of Salv1, an upstream Hippo pathway component[6]. Taken together, these studies solidify the Hippo pathway as a key signaling cascade for CM proliferation.

We sought a model system to explore the role of the Hippo pathway in cell density-dependent regulation of CM proliferation. It is difficult to study contact inhibition in vivo, where tight control of cell density is not possible. For example, acute mechanical perturbations followed by long-term live cell imaging are currently beyond available technologies. Therefore, we turned to in vitro models. It has previously been shown that plating low density human embryonic stem cell-derived CMs induces them to enter the cell cycle[20]. This was shown using

[1]Department of Cell and Developmental Biology, Vanderbilt University, Nashville, TN, USA. [2]Program in Developmental Biology, Vanderbilt University, Nashville, TN, USA. [3]Department of Biostatistics, Vanderbilt University Medical Center, Nashville, TN, USA. ✉email: dylan.burnette@vanderbilt.edu

flow cytometry to measure the expression of three cell cycle markers: BrdU, YAP, and cyclin D1. Furthermore, our previous work showed that human iPSC-derived CMs (hiCMs) are more proliferative when plated sparsely than when in a monolayer based on cell counting using high-content microscopy[21]. Whether the Hippo pathway regulates the apparent difference in CM-proliferation capacity in dense and sparse populations remains to be elucidated. This led us to probe whether the Hippo pathway is involved in regulating the proliferative capacity of CMs in various densities or if YAP is activated in these sparse populations by another mechanism. We have chosen hiCMs as our model system to study this phenomenon, as they are transcriptionally immature—similar to fetal or neonatal CMs in vivo—and have a slight basal proliferative capacity[22,23]. Here, we show that reducing hiCM density by either a scratch assay or by sparse plating increases nuclear YAP and CM-proliferation, and that this proliferative capacity can be further enhanced by combinatorial pharmacological perturbation of the Hippo pathway.

Results

Reducing hiCM density in a scratch assay increases proliferative capacity. We first investigated whether a reduction in hiCM density resulted in increased proliferation and/or any changes in Hippo pathway signaling. The hiCMs we used were purchased pre-differentiated and we confirmed the company's claim of a lack of fibroblast contamination (see "Materials and methods", Figure S1B) and slight proliferative capacity (Figure S1A,D,E)[21]. The lack of non-muscle cell types is key for interpretation of the data sets measuring proliferation. In addition, hiCMs can be cultured as a dense monolayer in which every cell has the potential to be experiencing contact inhibition.

One well-established method to relieve contact inhibition in culture is to scratch a confluent monolayer of cells[24]. Therefore, we used a micropipette tip to scratch a confluent monolayer of hiCMs (Fig. 1A,B). We hypothesized that, as in epithelial cells, YAP would translocate to the nucleus of hiCMs near the scratch, as these hiCMs should have reduced contact inhibition compared to those far from the scratch. To test this, we localized YAP using immunofluorescence 48 h post-scratch. We noticed that hiCMs near the edge of the scratch appeared to have primarily nuclear YAP (Fig. 1C). A proxy for YAP activity is to measure the nuclear accumulation of YAP[25]. Therefore, we acquired higher magnification images to measure the ratio of nuclear YAP to total YAP. We used β-catenin to mark adherens junctions between myocytes in order to delineate separate cells, and measured nuclear YAP and total YAP using fluorescence localization. We found that hiCMs near the scratch had a higher nuclear YAP to total YAP ratio than either hiCMs farther from the scratch on the same plate or hiCMs in an unscratched monolayer (Fig. 1C,D). Interestingly, this appeared to be an exponentially decaying relationship, where the nuclear YAP to total YAP ratio decreased rapidly as a function of distance from the scratch.

We next wanted to know if the increase in nuclear YAP correlated with an increase in hiCMs entering the cell cycle. One standard way to identify cycling cells is to localize Ki67 using immunofluorescence, as Ki67 is localized in the nuclei of cycling cells[26,27]. We found that in a monolayer of hiCMs, Ki67-positive cells were evenly distributed across the well and were found in actinin2- and troponinT-positive cells (Fig. 1E,F, Figure S1D,E). In contrast, for the scratched cells, there was a skewed distribution, in which more Ki67-positive nuclei were near the scratch (Fig. 1E,F). We further used the Fucci probe as evidence that cells near a scratch are cycling (Fig. 1G). Taken together, these data indicate that the relief of contact inhibition by a scratch assay increases the amount of YAP in the nuclei of hiCMs and promotes their entry into the cell cycle. However, it is worth noting that a scratch assay is inherently asymmetric as only hiCMs near a scratch respond, limiting measurements of responses on a population level. This further suggests that increase in cell proliferation is not entirely a paracrine mechanism. If a scratch induced cardiac myocyte proliferation in a nonautonomous fashion, all cells would undergo a similar increase in proliferation. While we cannot make the conclusion that in this system, the increase in nuclear YAP/total YAP ratio is directly causative of the increase in Ki67-positive nuclei near the scratch, we can conclude that the increase in proliferative capacity seen in a scratched monolayer of cardiac myocytes is at least in part cell autonomous.

Reducing hiCM density by sparse plating increases proliferative capacity. We next wanted to identify an assay that could model a uniform reduction in contact inhibition across an entire population of hiCMs. A previous study used flow cytometry and Western blotting to show that embryonic stem cell-derived cardiac myocytes begin cycling when they are sparsely plated[20]. Thus, we plated hiCMs as a monolayer or plated them sparsely. Not surprisingly, a monolayer of hiCMs (~ 1088 hiCMs/mm^2) have a low nuclear YAP/total YAP ratio (Fig. 2A,B). On the other hand, when cells are plated at an eightfold dilution (~ 136 hiCMs/mm^2), the nuclear YAP/total YAP ratio increases almost twofold (Fig. 2A,B).

This increase in nuclear YAP in sparsely-plated hiCMs suggested an increase in proliferative capacity. To test this, we asked if sparse plating caused entry into the cell cycle using Ki67 localization. We localized Ki67 in dense or sparse hiCMs and found an increase in Ki67-positive nuclei, indicating a near doubling in cycling hiCMs (Fig. 2C,D). We similarly used the Fucci probe system and found that the majority of dense hiCMs were not cycling, whereas sparse hiCMs had increased cycling cells (Fig. 2E). To directly test if sparse-plating induced proliferation in hiCMs, we counted the number of hiCMs over time. We found that while dense control hiCMs essentially remained the same over 48 h, there was a ~ 5% increase in the number of sparsely-plated hiCMs (Fig. 2F). Taken together, our data indicates that sparse plating induces hiCMs to enter the cell cycle and also divide. This led us to explore the underlying cause of sparsely-plated hiCMs to enter the cell cycle.

It has been postulated that CM division is preceded by dedifferentiation into a more immature phenotype[28,29]. Thus, we employed RNASeq analysis to examine whether the proliferating sparsely-plated hiCMs were as mature as hiCMs in a monolayer. We found CM-maturity genes (Table 1) were modestly downregulated in sparse hiCMs

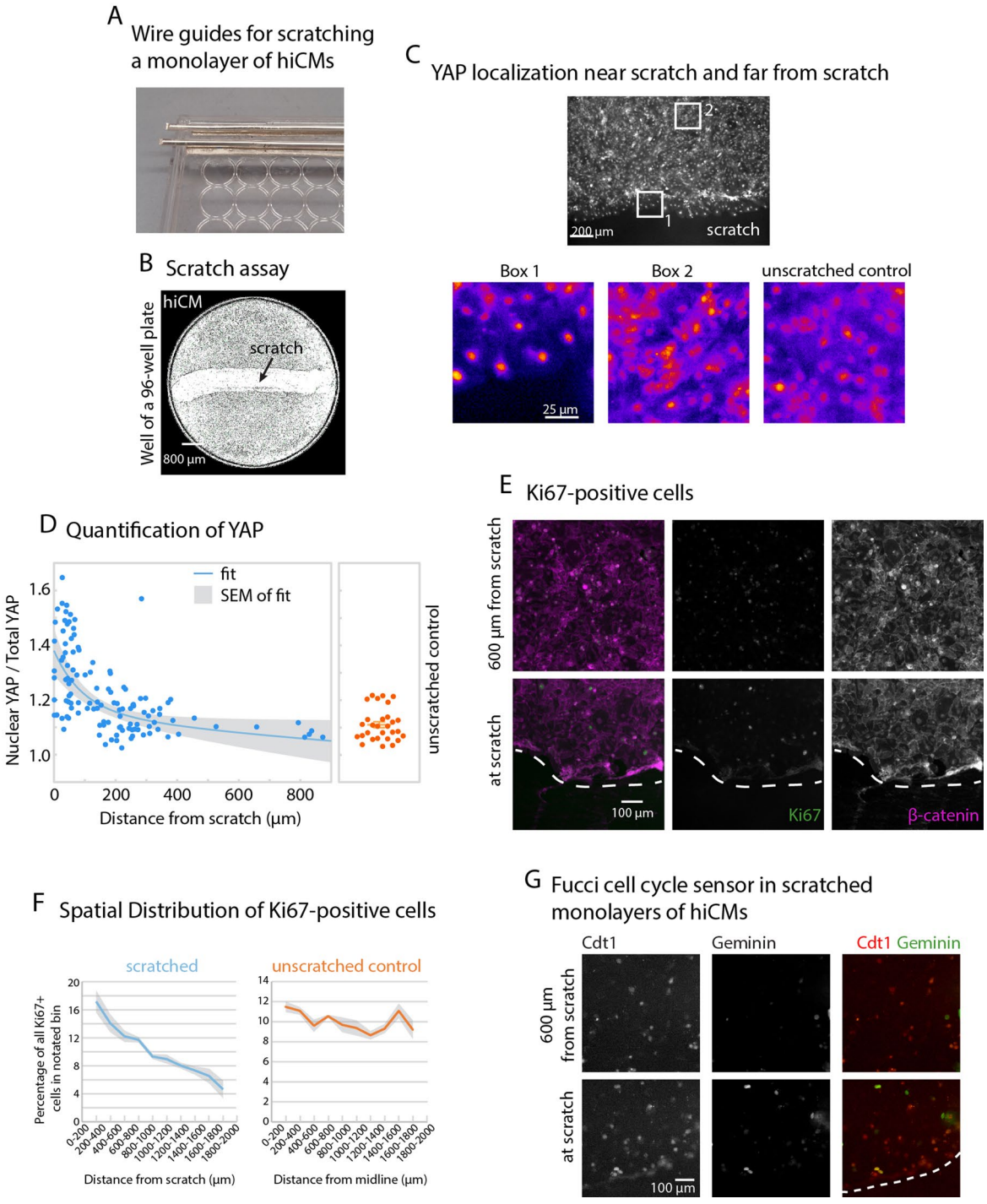

Figure 1. Reducing hiCM density by a scratch assay increases proliferative capacity. (**A**) Wire guide for scratching a monolayer of hiCMs, using a lid of a 96-well plate and a Dremel tool to drill through the plastic lid. Wire guides are composed of a bottom layer of flattened 21-gauge wire glued to the lid and a top layer of cylindrical wire to guide the pipette tip. (**B**) 4× whole-well phase-contrast image of hiCMs in a well of a 96-well plate, 48 h post-scratch. (**C**) YAP immunolocalization near the scratch (box 1) and far from the scratched (box 2) using 20× widefield microscopy. (**D**) Quantification of Nuclear YAP divided by total YAP (n = 79 cells from 5 independent experiments). Unscratched control (n = 29 cells from 3 independent experiments). (**E**) Ki67 and β-catenin in a scratched plate 48 h post-scratch using 20×. (**F**) Spatial distribution of Ki67-positive hiCMs in a scratched well or in an unscratched control well 48 h post-scratch. ***$p < 0.0001$, Chi-square = 80.434 with a two by five contingency table comparing distributions of Ki67 in different regions within 2 mm of the scratch or center of the midline of the well. (**G**) Fucci cell cycle probe transduced into a monolayer of hiCMs and scratched or not scratched.

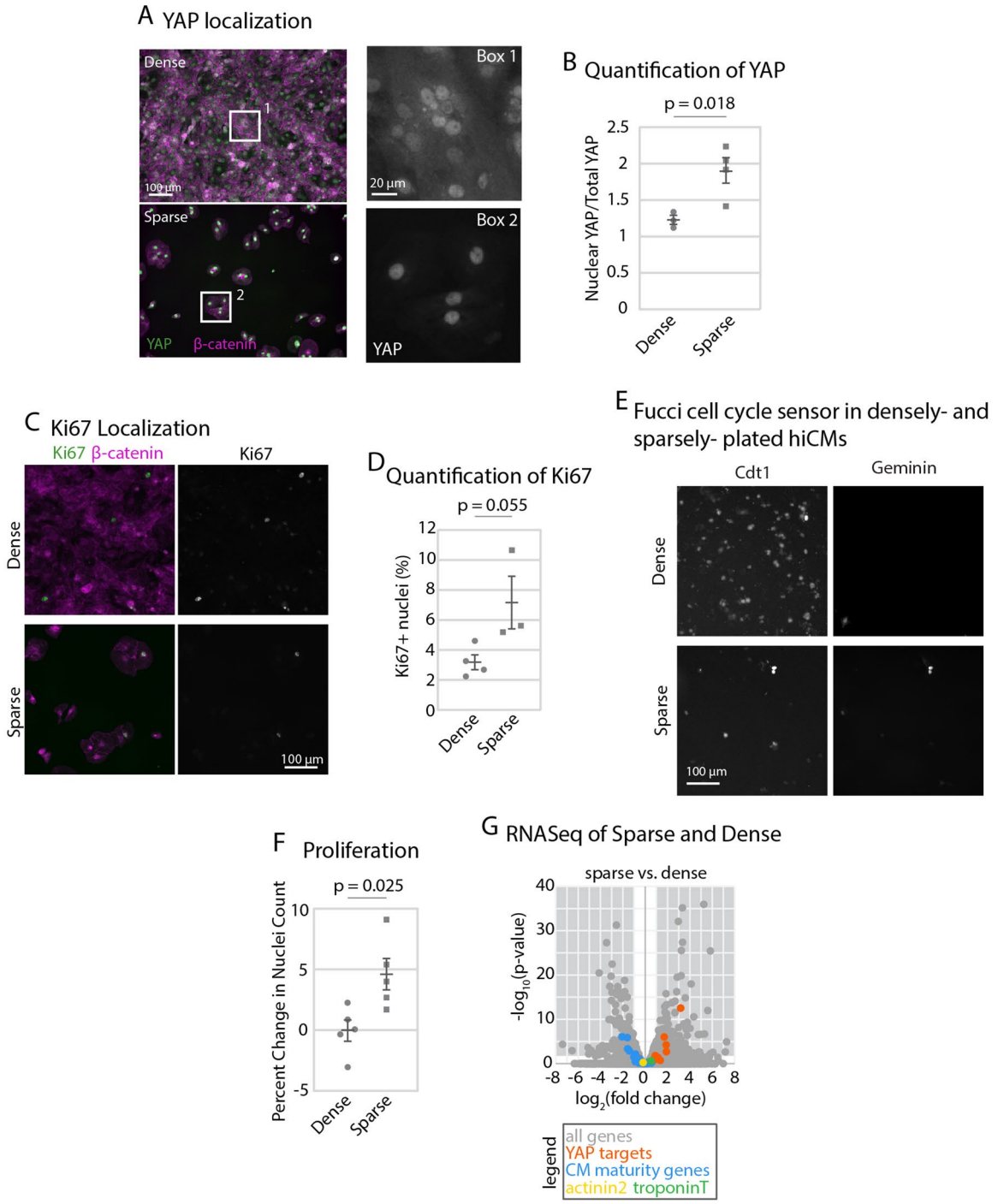

Figure 2. Reducing hiCM density by sparse plating increases proliferative capacity. (**A**) YAP and β-catenin in dense and sparse hiCMs using 20× widefield fluorescence microscopy. (**B**) Quantification of nuclear/total YAP ratio. Significance determined by paired two-tailed Student's *t* test. (N = 23 dense cells and 27 sparse cells from 3 independent experiments) (**C**) Ki67 and β-catenin immunolocalization in dense and sparse hiCMs using 20× widefield fluorescence microscopy. (**D**) Percent of Ki67-positive nuclei in dense (N = 8046 hiCMs from 4 experiments) and sparse (N = 1716 cells from 3 experiments) hiCMs. Significance determined by an unpaired two-tailed Student's *t* test. (**E**) Fucci cell cycle probe transduced into dense or sparse hiCMs. Arrows shows S–M phase. (**F**) Proliferation of dense or sparse hiCMs quantified by counting nuclei fold change over 48 h (N = 281,250 cells from 5 independent experiments). Significance determined by unpaired two-tailed Student's *t* test. (**G**) RNASeq Volcano plot of genes significantly changed in sparse versus dense hiCMs (N = 300,000 hiCMs per treatment from 3 independent experiments). A negative fold change represents a downregulation in sparse hiCMs. A positive fold change represents an upregulation in sparse hiCMs. Gene names of determined YAP target genes (including CTGF and CYR61), cardiac myocyte identity genes (TNNT2 and ACTN2), and cardiac myocyte maturity genes (including GATA4 and FOXOD) can be found in Tables 1, 2, 3.

Gene	Sparse (Dense) FC	p-value	XMU (Dense) FC	p-value	S1P (Dense) FC	p-value	XMU (Sparse) FC	p-value	S1P (Sparse) FC	p-value
CTGF	9.01	**2.89E−13**	25.81	**2.79 E−22**	17.62	**8.25 E−24**	2.93	**0.000134**	1.97	**0.007319**
GADD45G	3.73	**0.002072**	6.56	**0.000193**	10.85	**0.000115**	1.79	0.605755	3.00	**0.038005**
CYR61	3.66	**5.95 E−05**	10.82	**1.04 E−13**	6.92	**6.18 E−14**	3.01	**0.000925**	1.91	**0.020171**
GADD45B	3.26	**9.59 E−07**	5.54	**1.41 E−08**	4.45	**0.001261**	1.74	0.126936	1.39	0.36164
GLI2	1.53	0.393604	3.82	**6.2 E−22**	2.24	0.185947	2.54	**0.004467**	1.47	0.316052
CDKN2B	2.54	0.175283	2.99	**0.000286**	2.57	0.384279	1.22	0.792722	1.01	0.983649
MYC	2.11	0.065524	3.30	**9.61 E−08**	3.98	**7.42 E−08**	1.60	0.275537	1.90	**0.012205**
VIM	1.85	**0.026872**	1.39	**0.000517**	1.68	**0.038557**	0.77	0.478305	0.92	0.7466
TEAD4	1.87	**0.015487**	1.63	**9.48 E−06**	1.68	**0.023656**	0.89	0.778883	0.91	0.679315
GPATCH4	2.18	**0.038921**	0.78	0.115272	2.01	0.357642	0.37	**0.002401**	0.93	0.87144
TXN	1.69	0.183088	1.36	**0.039324**	1.96	0.299241	0.82	0.697661	1.18	0.672179
CAV1	0.63	0.143092	0.33	**4.8 E−18**	0.62	0.135195	0.53	**0.004174**	1.00	0.99217
CAT	0.81	0.520764	0.84	0.245518	0.73	0.551213	1.06	0.871611	0.90	0.656182
TEAD1	1.08	0.904655	1.70	**3.93 E−06**	1.31	0.694522	1.61	0.246832	1.21	0.571363
AXL	0.71	0.199238	0.62	**0.000225**	0.70	0.260978	0.88	0.69564	0.99	0.962445
CCND1	1.21	0.480377	0.99	0.95182	1.15	0.630965	0.83	0.467474	0.96	0.791495
ERBB4	0.82	0.630638	0.95	0.814267	1.01	0.995008	1.18	0.703516	1.22	0.533846
WSB2	0.91	0.780978	0.81	**0.033037**	0.82	0.757739	0.90	0.726643	0.90	0.696159
LMNB2	1.12	0.807049	0.97	0.900838	1.08	0.886014	0.89	0.761298	0.97	0.88176
TNFAIP3	0.74	0.686538	0.35	**0.000508**	0.50	0.405358	0.48	0.239423	0.68	0.417583
GATA6	0.67	0.057851	0.65	**1.49 E−07**	0.68	0.083787	0.98	0.965776	1.02	0.936819
PLK2	0.72	0.112915	0.41	**2.48 E−06**	0.64	**0.002456**	0.58	0.142406	0.90	0.570129
YAP	1.00	0.998472	0.83	**0.025910**	0.97	0.959423	0.84	0.681629	0.97	0.999937
TAZ	1.36	0.720522	0.50	**0.002689**	0.55	0.126824	0.37	0.111599	0.41	0.999937
MST1	0.86	0.802404	0.95	0.870735	0.68	0.528100	1.12	0.804197	0.80	0.999937
MST2	1.19	0.640836	0.95	0.870735	1.02	0.977948	1.06	0.904359	0.86	0.999937
LATS1	0.74	0.544618	1.17	0.283387	0.95	0.947461	1.62	0.241345	1.29	0.999937
LATS2	1.00	0.999502	1.97	**1.01 E−12**	1.14	0.893674	2.01	**0.010439**	1.14	0.999937

Table 1. RNASeq results of YAP target gene expression. *FC* fold change. The comparisons are made between the first treatment (outside of the parentheses, listed first) and the second (Inside the parentheses). A fold change greater than 1 indicates in increase in gene expression in the first treatment type compared to the second, and a fold change greater than 1 indicates a decrease in gene expression in the first treatment type compared to the second. p-values were obtained as in the methods. Bold values indicate significant differences

(Fig. 2G)[22]. However, expression of CM-identity genes α-actinin 2 and troponinT did not change (Fig. 2G; Table 3). Thus, sparsely-plated hiCMs are less mature than densely-plated hiCMs, but they remain CMs.

We next wanted to test if the increase in nuclear YAP ratio in sparsely-plated hiCMs was correlated with higher YAP target gene expression. Thus, we curated a list of YAP target genes from the published literature[30–32]. We then compared the expression of these genes between densely-plated and sparsely-plated hiCMs. 32% of YAP target genes had upregulated expression in sparsely-plated hiCMs compared to dense, while 68% did not change, and 0% had decreased expression. In conclusion, plating hiCMs sparsely increases YAP nuclear localization, YAP target gene expression, and ultimately, hiCM proliferation compared to densely-plated hiCMs.

Pharmacological perturbation of the Hippo pathway affects cardiac myocyte proliferation. A loss of contact inhibition not only increased hiCM proliferation but also the nuclear YAP/total YAP ratio, consistent with the hypothesis that the Hippo pathway is involved in density-dependent hiCM proliferation. We next asked if small molecule inhibition of the Hippo pathway would further increase the proliferative potential of hiCMs plated at a low density. We turned to an MST1/2 inhibitor, XMU-MP-1, and a bioactive lipid that activates YAP, sphingosine-1-phosphate (S1P)[23,33,34] (Fig. 3A). Both of these compounds have been shown to upregulate YAP target genes in human embryonic stem cells, mouse liver cells and human hepatoma cells[30,33]. Furthermore, S1P increases Ki67 in densely plated hiCMs but not cell count when combined with lysophosphatidic acid[23].

We used RNASeq analysis to test if XMU-MP-1 or S1P upregulate YAP/TAZ target genes in hiCMs, and found that YAP/TAZ target genes were indeed significantly upregulated beyond that of sparse-plating alone (Fig. 3B; Table 1). This increase in YAP target gene expression suggests that the compound-treated hiCMs are less mature than untreated sparsely-plated hiCMs. We found that S1P treatment did not lower the expression of maturity genes compared to untreated hiCMs, whereas 4.2% of maturity genes were expressed lower after XMU-MP-1 treatment (Fig. 3C; Table 2). We then confirmed that the hiCMs were still expressing CM specific markers

Gene	Sparse (Dense) FC	p-value	XMU (Dense) FC	p-value	S1P (Dense) FC	p-value	XMU (Sparse) FC	p-value	S1P (Sparse) FC	p-value
KLF15	0.37	**0.001345**	0.62	**0.015381**	0.40	0.081736	1.69	0.216003	1.08	0.852327
PPARA	0.50	**0.033375**	0.69	**0.000397**	0.51	0.059213	1.42	0.404501	1.04	0.913521
RB1	0.66	0.377255	1.07	0.637022	0.80	0.801415	1.65	0.23275	1.21	0.62234
RXRA	0.67	0.183603	0.75	**0.008464**	0.66	0.090851	1.15	0.740298	1.00	0.995685
PPARGC1A	0.69	0.237739	0.46	**2.62 E−09**	0.75	0.403987	0.69	0.305008	1.10	0.703669
NUPR1	0.67	0.718043	0.03	**0.00025**	1.33	0.902237	0.05	0.065356	2.04	0.421311
PPARD	0.72	0.091847	0.88	0.254178	0.65	0.407204	1.25	0.360958	0.90	0.70345
STAT5B	0.96	0.925941	1.30	**0.005076**	0.88	0.835451	1.38	0.238056	0.92	0.749992
TP53	1.04	0.919216	0.74	**0.007432**	1.17	0.620798	0.73	0.178197	1.13	0.501919
SMARCA4	1.38	0.318031	1.07	0.563766	1.37	0.427076	0.79	0.484057	1.01	0.984053
PPARGC1B	0.57	0.118278	0.24	**3.94 E−19**	0.70	0.255304	0.43	**0.02966**	1.24	0.451305
SIRT1	0.64	0.391808	1.17	0.300566	0.70	0.460866	1.85	0.167862	1.10	0.785253
BRCA1	0.70	0.444602	0.39	**5.06 E−07**	0.68	0.240951	0.57	0.255112	0.97	0.929278
ISL1	0.70	0.72808	0.39	**0.047124**	1.27	0.832355	0.57	0.575785	1.85	0.226337
EZH2	0.95	0.925928	0.90	0.608155	0.99	0.989079	0.97	0.957506	1.04	0.872184
KLF2	1.07	0.943608	2.03	0.307754	1.36	0.80982	1.93	0.374266	1.31	0.606284
TCF7L2	1.11	0.804331	0.82	0.208738	1.40	0.432616	0.75	0.257579	1.28	0.274109
IRF3	1.22	0.675849	1.29	**0.038872**	1.26	0.749532	1.08	0.891222	1.05	0.881247
EPAS1	0.33	**1.33 E−06**	0.34	**1.38 E−16**	0.23	**0.015726**	1.04	0.945471	0.69	0.436981
STAT6	0.55	**0.006801**	0.19	**2.02 E−30**	0.37	**0.000199**	0.35	**2.87 E−05**	0.68	0.125648
HMGA1	0.71	0.242416	0.72	**0.000562**	0.74	0.087149	1.04	0.929241	1.05	0.807651
CREBBP	0.76	0.429739	0.98	0.906761	0.94	0.893223	1.32	0.408709	1.24	0.3625
RORA	0.77	0.632319	1.10	0.719185	0.81	0.681446	1.44	0.432174	1.05	0.881326
TBX5	0.81	0.516316	0.73	**0.015109**	0.88	0.818683	0.91	0.753349	1.09	0.682947
HIF1A	0.91	0.827102	0.73	**0.000624**	0.88	0.888031	0.82	0.57784	0.98	0.944643
ESRRA	0.97	0.964559	0.64	**0.001142**	0.66	0.201523	0.67	0.165544	0.69	0.080643
GATA4	0.97	0.924665	1.54	**8.22 E−09**	1.08	0.894736	1.62	**0.002196**	1.12	0.607182
MEF2C	1.07	0.85549	1.26	**0.043804**	1.51	**0.008506**	1.20	0.525246	1.42	0.054329
MYOCD	1.22	0.587856	0.84	0.148871	1.24	0.38708	0.70	0.236397	1.02	0.931564
SREBF1	0.34	**0.00046**	0.32	**1.42 E−11**	0.40	**0.00197**	0.96	0.945008	1.18	0.522472
NR2C2	0.54	0.352976	0.94	0.749191	0.62	0.730363	1.77	0.374012	1.14	0.829856
EP300	0.70	0.467532	1.15	0.234023	0.85	0.847678	1.66	0.220495	1.21	0.612428
FOXO3	0.75	0.349721	0.86	0.130914	0.78	0.216367	1.17	0.641334	1.05	0.805169
CEBPB	0.94	0.922627	0.88	0.386107	1.17	0.797417	0.96	0.952266	1.27	0.462195
AHR	0.93	0.932517	1.35	0.172625	1.00	0.998442	1.46	0.403747	1.07	0.848077
ESRRA	0.97	0.964559	0.64	**0.001142**	0.66	0.201523	0.67	0.165544	0.69	0.080643
TFAM	0.98	0.972321	0.93	0.638489	1.12	0.815031	0.96	0.925733	1.15	0.524921
TCF3	1.07	0.870547	1.03	0.829302	0.99	0.976384	0.98	0.966962	0.93	0.718576
NR4A3	1.11	0.880451	4.19	**0.042536**	2.08	0.097711	3.84	**0.020697**	1.89	**0.035762**
NFATC2	0.24	**8.81 E−07**	0.31	**4.36 E−14**	0.45	**0.01823**	1.33	0.590606	1.85	0.066561
TOB1	0.69	0.202871	0.71	**0.006508**	0.64	**0.047766**	1.05	0.921464	0.93	0.750685
CTCF	0.77	0.330234	0.91	0.388474	0.73	0.337073	1.20	0.520739	0.95	0.79525
HDAC1	0.93	0.868417	1.14	0.307232	0.80	0.595919	1.25	0.423766	0.86	0.476421
E2F6	0.98	0.964822	1.04	0.850897	0.98	0.95372	1.08	0.834633	1.00	0.980775
GMNN	1.01	0.983859	0.77	0.075827	1.04	0.948911	0.78	0.420264	1.04	0.882408
USF1	1.19	0.652289	1.01	0.9356	1.18	0.807159	0.87	0.699954	1.01	0.985944
STAT5A	1.44	0.745261	0.72	0.622383	0.71	0.869697	0.51	0.548587	0.49	0.406925
ATF3	1.39	0.496897	6.55	**0.001271**	4.69	**3.45 E−13**	4.80	**0.001356**	3.44	**3.16 E−05**

Table 2. Cardiomyocyte maturity genes. Bold values indicate significant differences

(Fig. 3B; Table 1). Taken together, our data indicates that XMU-MP-1 or S1P treatment causes an upregulation of YAP/TAZ target genes with minor effects on maturity of hiCMs.

Despite an upregulation in YAP/TAZ target genes, we found that neither XMU-MP-1 nor S1P alone increased proliferation by hiCM count (Fig. 3D). The result that XMU-MP-1 or S1P failed to induce proliferation was not

Gene	Sparse (Dense) FC	p-value	XMU (Dense) FC	p-value	S1P (Dense) FC	p-value	XMU (Sparse) FC	p-value	S1P (Sparse) FC	p-value
ACTN2	0.88	0.59668	0.91	0.278626	0.86	0.683813	1.05	0.874083	0.98	0.913769
TNNT2	1.46	0.250773	1.05	0.770643	1.37	0.735052	0.74	0.400782	0.96	0.915476

Table 3. Cardiomyocyte-specific genes.

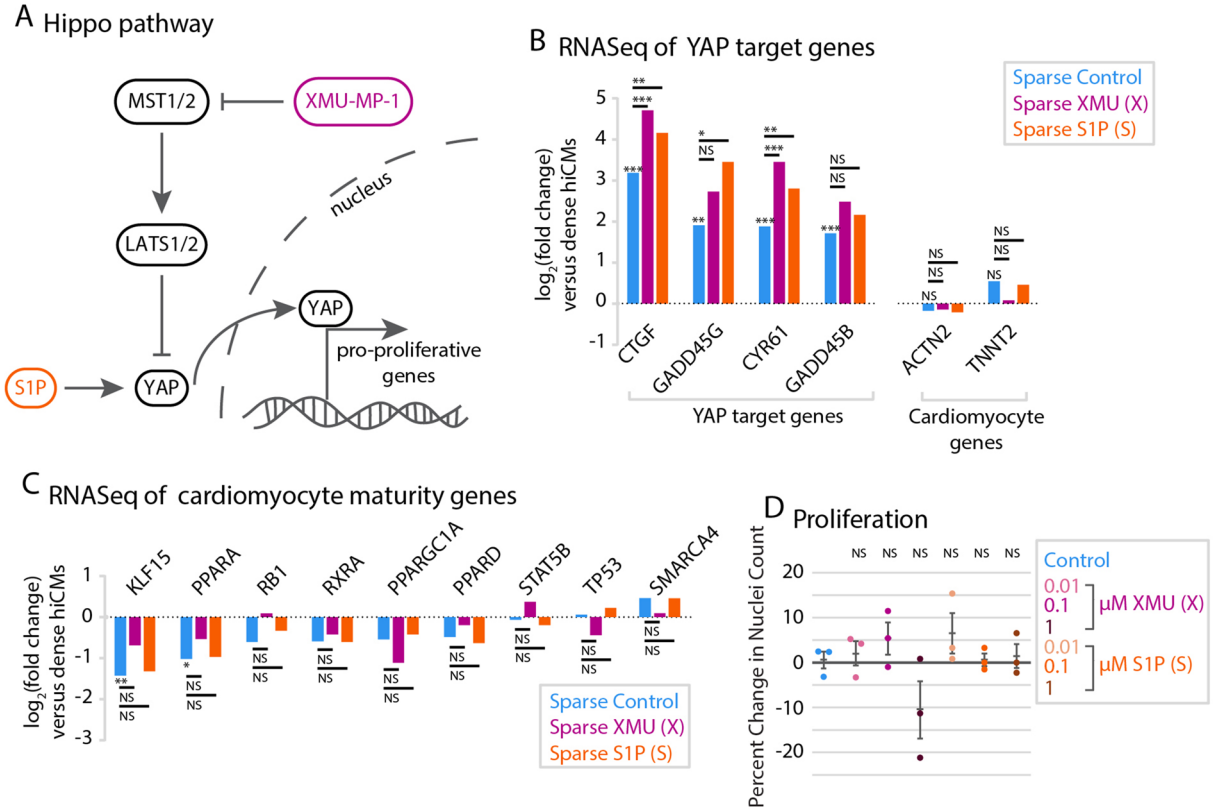

Figure 3. Individual pharmacological perturbation of the Hippo pathway increases YAP target genes but does not affect proliferation. (**A**) Schematic of the Hippo pathway. (**B**) RNASeq data of YAP target genes in sparse cells with treatment of 1 μM XMU-MP-1 or 1 μM S1P. A negative fold change represents a downregulation in treated cells, whereas a positive fold change represents an upregulation in treated cells. N = 300,000 cells per treatment, over 3 independent experiments and RNA preparations. Right: cardiac myocyte-specific genes do not change upon small molecule treatment. *$p < 0.05$, **$p < 0.01$, ***$p < 0.001$. All p-values and gene names are available in Tables 1, 2, 3. Differentially expressed genes were determined using the criteria of fold change ≥ 2 and FDR ≤ 0.05. (**C**) RNASeq data of CM-maturity genes as in (**B**). (**D**) Quantification of proliferation of control, XMU-MP-1-, and S1P-treated cells by measuring the percent change in nuclei over 48 h post-treatment. Significance determined by one-way ANOVA with a Dunnett's post-hoc test corrected for multiple testing.

surprising, as previous studies have postulated that combinations of multiple genetic or pharmacological factors are required to induce cardiac myocyte proliferation both in vitro and in vivo[35,36]. Therefore, we performed a combinatorial screen to determine if combining XMU-MP-1 and S1P induced proliferation of hiCMs. We started by testing which combination of concentrations was most effective to induce hiCMs to reenter the cell cycle using BrdU incorporation (Fig. 4A). We found that adding 0.1 μM of each compound to hiCMs significantly increased the percent of BrdU-positive hiCMs when sparsely-plated (Fig. 4B). We then found that this combination significantly increased hiCM-proliferation by counting nuclei over time (Fig. 4C). We found that using 0.1 μM of both XMU-MP-1 and S1P also decreased phospho-YAP, which indicated a reduction in the inactivation of YAP (Fig. 4D–F).

It is important to confirm that these proliferative hiCMs are functionally beating upon treatment of XMU-MP-1 and S1P. Therefore, we measured the percentage of beating hiCMs upon sparse plating and treatment of XMU-MP-1, S1P, or both, and found no significant difference (Fig. 4G). Further, it is important to consider that both cytokinetic cell division and binucleation are potential outcomes of increasing overall proliferation of cells. We measured the percentage of binucleated hiCMs upon sparse plating and treatment of XMU-MP-1, S1P, or both, and found no significant difference (Fig. 4H). In this case, it is presumed that proliferation appears to be induced overall, but the balance between the potential outcomes of cell division and binucleation are not

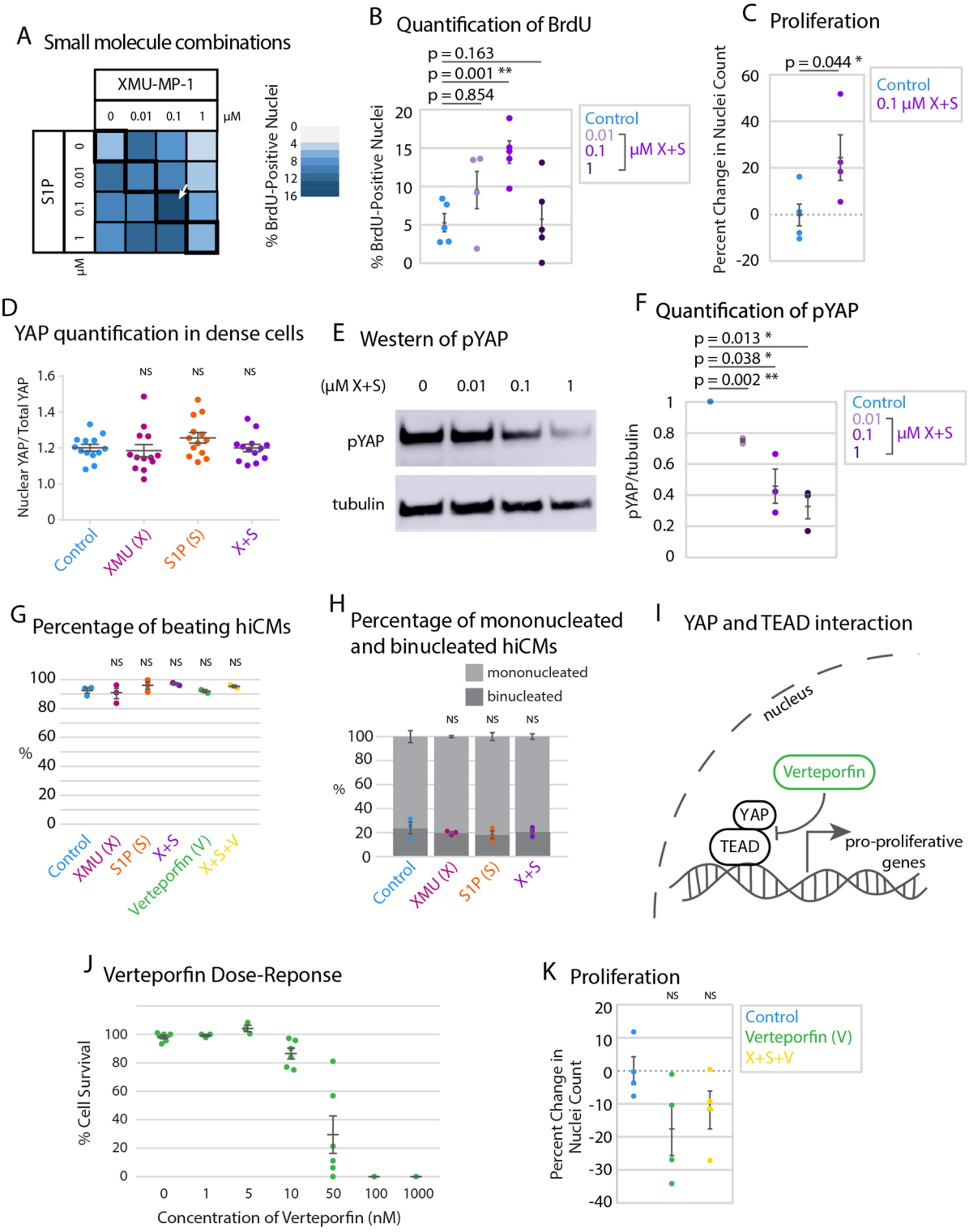
A
Small molecule combinations
XMU-MP-1
0 0.01 0.1 1 μM
S1P
0 0.01 0.1 1 μM
% BrdU-Positive Nuclei
0 4 8 12 16
B
Quantification of BrdU
p = 0.163
p = 0.001 **
p = 0.854
% BrdU-Positive Nuclei
Control
0.01
0.1
1
μM X+S
C
Proliferation
p = 0.044 *
Percent Change in Nuclei Count
Control
0.1 μM X+S
D
YAP quantification in dense cells
Nuclear YAP/ Total YAP
NS NS NS
Control
XMU (X)
S1P (S)
X+S
E
Western of pYAP
(μM X+S) 0 0.01 0.1 1
pYAP
tubulin
F
Quantification of pYAP
p = 0.013 *
p = 0.038 *
p = 0.002 **
pYAP/tubulin
Control
0.01
0.1
1
μM X+S
G
Percentage of beating hiCMs
NS NS NS NS NS
%
Control
XMU (X)
S1P (S)
X+S
Verteporfin (V)
X+S+V
H
Percentage of mononucleated and binucleated hiCMs
mononucleated
binucleated
NS NS NS
%
Control
XMU (X)
S1P (S)
X+S
I
YAP and TEAD interaction
nucleus
Verteporfin
YAP
TEAD
pro-proliferative genes
J
Verteporfin Dose-Reponse
% Cell Survival
0 1 5 10 50 100 1000
Concentration of Verteporfin (nM)
K
Proliferation
NS NS
Percent Change in Nuclei Count
Control
Verteporfin (V)
X+S+V

◂**Figure 4.** Combination of XMU-MP-1 and S1P increases cardiac myocyte proliferation. (**A**) Heat map showing percentage of BrdU-positive nuclei in a preliminary screen of combinatorial treatment of hiCMs with XMU-MP-1 and S1P. N = 8393 cells from 5 independent experiments. (**B**) BrdU+ datapoints from black outlined diagonal center boxes from heat map. N = 2229 cells from 5 independent experiments. (**C**) Proliferation of control hiCMs or 0.1 μM XMU-MP-1 and 0.1 μM S1P-treated cells measured by counting nuclei over 48 h. N = 17,318 DMSO-treated cells and 16,234 XS-treated cells from 4 independent experiments. Significance determined by two-tailed paired Student's *t* test. (**D**) Western blot of hiCMs treated with various concentrations of both XMU-MP-1 and S1P. pYAP: phosphorylated YAP (see Figure S1F,G for the entire blot). (**E**) pYAP amount in hiCMs measured by western blot normalized to tubulin (N = 3 independent experiments). (**F**) The compounds XMU-MP-1, S1P, and Verteporfin do not affect the percentage of beating hiCMs at the doses given (1 μM for XMU-MP-1 and S1P, 0.1 μM for XMU-MP-1 and S1P combined, and 10 nM Verteporfin. In last row, 0.1 μM of XMU-MP-1 and S1P were combined with 10 nM Verteporfin). (**G**) The compounds XMU-MP-1 and S1P do not affect the percentage of binucleated and mononucleated hiCMs at the same doses as (**F**). (**H**) Schematic of YAP's downstream transcriptional regulation and interaction with TEAD. (**I**) Verteporfin dose response to detect which concentration of Verteporfin inhibited hiCM proliferation, but did not lead to massive cell death. (**J**) Proliferation of control hiCMs compared to 0.01 μM Verteporfin, or 0.01 μM Verteporfin, 0.1 μM S1P, and 0.1 μM XMU-MP-1-treated hiCMs. N = 1257 cells from 4 independent experiments. (**K**) Proliferation of control hiCMs compared to 0.01 μM Verteporfin, or 0.01 μM Verteporfin and 0.1 μM S1P, and 0.1 μM XMU-MP-1-treated hiCMs. Significance determined by one-way ANOVA with a Dunnett's post-hoc test correcting for multiple testing for panels (**B**), (**E**), (**F**), (**G**), and (**J**).

changed, and both outcomes are occurring. These results agree with past research inducing hiCMs to divide, showing both binucleation and cell division as outcomes[21].

Finally, to further confirm that XMU-MP-1 and S1P were acting through the Hippo pathway, we turned to Verteporfin, which inhibits the interaction of YAP with transcription factor TEAD[37] (Fig. 4I). For this experiment we chose 0.01 μM of Verteporfin, which is the highest concentration that did not result in the death of hiCMs (Fig. 4J). We found that Verteporfin masked the effect of the combination of XMU-MP-1 and S1P combination on proliferation (Fig. 4K) without affecting the percentage of beating hiCMs (Fig. 4G). This result further suggests that the increase in proliferation of hiCMs with XMU-MP-1 combined with S1P is through the Hippo pathway.

Discussion

Taken together, we show that the density at which hiCMs are plated affects proliferative capacity, and that this proliferative capacity is regulated at least in part by the Hippo pathway. Further, we modulate the proliferative capacity by scratching a monolayer of cells to induce cells at the scratch periphery to divide, and induce division of sparsely-plated hiCMs by dual inhibition of the Hippo pathway. These experiments were completed using hiCMs, a model system of developmentally immature cells that both divide and binucleate, providing an ideal model for studying cardiomyocyte division. This is an alternative approach to using isolated primary cardiomyocytes from adult rats or mice, which are unsuitable to the experiments we use here. While primary cardiomyocytes are powerful tools, creating dense monolayer is technically challenging. In addition, primary cardiomyocytes only last a few days in culture and are more representative of modeling cell death[38]. Therefore, it is difficult to do contact inhibition studies and proliferative studies in these cell types. As we show here, hiCMs are well suited for these types of studies[21].

It is not surprising that XMU-MP-1 itself did not increase CM proliferation, as a recent study found that XMU-MP-1 in an intact heart did not increase Ki67 staining[39]. Based on Ki67 staining, recent data has also suggested that inhibiting the Hippo pathway with a single compound in combination with perturbation of another cell cycle pathway (i.e., the Wnt pathway) could be an effective approach to increasing CM proliferation[35]. Here, we show that it is possible to have a combinatorial effect on CM proliferation by only targeting the Hippo pathway. Modulation of the Hippo pathway at two different levels was required to get a proliferative response. This could be part of a new direction for combinatorial therapy, where multiple pathways are each modulated at multiple levels.

There are several other pathways that drive CM proliferation. A recent study suggests the neuregulin receptor, ERBB2, activates YAP in an ERK-dependent manner[40]. The role of ERK signaling in cardiomyocyte proliferation and its crosstalk with the Hippo pathway would constitute an interesting future study. Furthermore, the signaling role that cell–cell adhesions and junctions themselves play in the cardiac regenerative response seems to merge on these pathways. Regenerating cardiac myocytes undergo junction dissolution, and it has been shown that displaced alpha-catenin activates YAP in epidermal cells[15]. Finally, increasing YAP and TAZ activity is likely to have benefits in the heart other than increasing cardiac myocyte proliferation. For example, YAP and TAZ in the epicardium was shown to induce recruitment of T-regulatory cells to the infarcted myocardium. Thus, YAP and TAZ may have the ability to regulate the adaptive immune response and decreasing post-infarct inflammation and myocardial fibrosis[41].

Finally, our work also has implications in the context of a myocardial infarction. In the developed heart, a myocardial infarction results in massive CM death and the remaining CMs do not proliferate[42]. After a myocardial infarct, there is a reduction in cell density at the infarct zone with an increase in cell cycling shown by Ki67 fluorescence[43]. However, it has been shown that the proliferative cells in the infarct region appear to mostly undergo polyploidization and endomitosis, indicating that there is a reduction in contact inhibition but there is also still a barrier to true cytokinetic proliferation in this region. Interestingly, YAP is primarily nuclear in the border zone 21 days post-cardiac apex resection, but only in *Salv* CKO animals[44]. If an ideal treatment for a cardiac infarction existed, it would only induce proliferation at the infarct site where cell–cell contact is reduced. Global

induction of proliferation could induce undesired side effects (e.g. tumor formation). As such, targeting pathways which respond preferentially when contact inhibition is lost could be a useful therapeutic direction. Here, we show that targeting the Hippo pathway can increase proliferation in the context of a loss of contact inhibition.

Materials and methods

Key resources.

Reagent or resource	Source	Identifier
Antibodies		
Mouse-anti-α-actinin-2	Sigma	A7811 Clone: EA53
Mouse anti-β-catenin	BD Biosciences	610153
Rabbit-anti-YAP	Cell Signaling Technologies	14074T
Rabbit-anti-phosphoYAP	Cell Signaling Technologies	13008S
Mouse-anti-α-tubulin	Sigma	B512 Clone: DM1α
Rabbit-anti-Ki67	Cell Signaling Technologies	9129S
Mouse-anti-BrdU	Cell Signaling Technologies	5292
Mouse-anti-TroponinT	Developmental Studies Hybridoma Bank	CT3
Goat anti-mouse 488	LifeTechnologies	A11001
Goat anti-rabbit 488	LifeTechnologies	A11034
Goat anti-mouse 568	LifeTechnologies	A11004
Goat anti-rabbit 568	LifeTechnologies	A11036
Goat anti-mouse HRP	LifeTechnologies	62-6520
Goat anti-rabbit HRP	LifeTechnologies	65-6120
Biological samples		
Cardiac myocytes[2]	Cellular Dynamics	CMC-100-012-000.5
Bovine Serum Albumin	RPI	A30075-100.0
Chemicals, peptides, and recombinant proteins		
NucLight Rapid Red	Essen Biosciences	4717
Vectashield with DAPI	Vector	H-1200
Cardiac myocyte Plating Medium	Cellular Dynamics	M1001
Cardiac myocyte Maintenance Medium	Cellular Dynamics	M1003
PBS, 10×, Ca^{2+}/Mg^{2+} free	Gibco	70011-044
Paraformaldehyde, 16%	Electron Microscopy Sciences	15710
PBS, 10×, with Ca^{2+}/Mg^{2+}	Corning	46-013-CM
0.5% Trypsin	Gibco	15400-054
0.1% Gelatin	Sigma	ES-006-B
Dimethyl Sulfoxide	Sigma	276855
Triton X-100	Fisher Scientific	BP151100
Fibronectin	Corning	354008
BrdU	Abcam	Ab142567
XMU-MP-1	SelleckChem	S8834
S1P	Apex Bio	B6707
Methanol	Fisher Scientific	A452SK-1
Verteporfin	Sigma	SML0534
Premo FUCCI Cell Cycle Sensor	Invitrogen	P36238
Software and Algorithms		
FIJI/ImageJ	NIH, Open Source	
Incucyte analysis software	Essen Biosciences	
MATLAB	MathWorks	

Cardiac myocyte culture and chemicals. iPSC-derived human cardiac myocytes (hiCMs, Cellular Dynamics, Madison, WI) were seeded as per manufacturer's instructions in cardiac myocyte plating medium (M1001, Cellular Dynamics, Madison, WI) in polystyrene 96-well cell culture plates coated in 0.1% sterile gelatin (ES-006-B, Sigma Aldrich, St. Louis, MO). Approximately 50,000 cells were seeded for dense plating and 6250 cells for sparse plating (1:8), and were subsequently cultured in cardiac myocyte maintenance medium (M1003, Cellular Dynamics, Madison, WI). These cells are verified by Cellular Dynamics (Madison, WI), and each vial of cells is tested at the company for purity by cTNT+ cells using flow cytometry (over 99% pure), identity using SNP genotyping, mycoplasma testing by PCR, sterility testing by 21 CFR 610.12, MEA functionality testing by

field potential duration and beating rate, and viability by trypan blue exclusion. We further characterized these cells in Neininger et al., 2019, in which we determined that fewer than 1 in 50,000 cells were actinin2-negative[21].

Cells were kept at 37 °C and 5% CO_2. For re-plating experiments, hiCMs were washed 2 × with 100 µL 1 × PBS with no Ca^{2+}/$Mg2^{2+}$ (PBS*, 70011-044, Gibco, Grand Island, NY). PBS* was completely removed from hiCMs and 40 µL 0.1% Trypsin–EDTA with no phenol red (15400-054, Gibco, Grand Island, NY) was added to hiCMs and placed at 37 °C for 2 min. Following incubation, culture dish was washed 3 × with trypsin inside well, rotated 180°, and washed another 3 ×. Trypsinization was then quenched by adding 120 µL of culture media and total cell mixture was placed into a 1.5 mL Eppendorf tube. Cells were spun at 1000*g* for 3 min, and supernatant was aspirated. Cells were then re-suspended in 200 µL of culture media and plated into 2 wells, 100 µL each, on a standard polystyrene 96-well cell culture plate (3599, Corning, Corning, NY) previously coated with 10 µg/mL Fibronectin (#354008, Corning, Mannassas, VA) for 1 h at 37 °C.

XMU-MP-1 (S8334, Selleck Chemicals, Houston, TX) and Verteporfin (SML0534, Sigma Aldrich, St. Louis, MO) were reconstituted to 10 mM in DMSO. S1P (B6707, Apex Bio, Houston, TX) was reconstituted to 10 mM in methanol. When adding drugs to the cells, they were first diluted 1:10 in DMSO then to the appropriate concentration in cardiac myocyte maintenance medium. NucLight Rapid Red Reagent (4717, Essen BioScience, Ann Arbor, MI) was used at a 1:4000 dilution in cell culture media.

Fixation and immunostaining. Cells were fixed with 4% paraformaldehyde (PFA, 15710, Electron Microscopy Sciences, Hatfield, PA) diluted form 16% in PBS at room temperature for 20 min, then extracted for 5 min with 1% Triton X-100 (BP151100, Fischer Scientific, Suwanee, GA) and 4% PFA in PBS. Cells were washed three times in 1 × PBS. After fixation, the following labeling procedures were used: for immunofluorescence experiments, cells were blocked in 10% bovine serum albumin (BSA) in PBS for 20 min. Primary antibodies were diluted in 10% BSA. All primary antibodies were used at 1:200 for 1 h and 45 min at room temperature. Secondary antibodies were diluted in 10% BSA at 1:100 and centrifuged at 13,000 rpm for 2 min before use at room temperature for 1 h.

Mouse anti-β-catenin was purchased from BD Biosciences (610153). Rabbit anti-Ki67 (9129S) and Rabbit anti-YAP (14074T) were purchased from Cellular Signaling Technologies (Danvers, MA). Mouse anti-actinin-2 (a7811) was purchased from Sigma Aldrich (St. Louis, MO). Rabbit anti-phosphoYAP (13008S) was purchased from Cellular Signaling Technologies (Danvers, MA). Mouse anti-BrdU (5292S) was purchased from Cellular Signaling Technologies (Danvers, MA). Alexa Fluor 488-goat anti-mouse (A11029), Alexa Fluor 488-goat anti-rabbit (A11034), Alexa Fluor 568-goat anti-rabbit (A11011), and Alexa Fluor 568-goat anti-mouse (A11004) antibodies were purchased from Life Technologies (Grand Island, NY).

BrdU (ab142567, abcam, Cambridge, UK) was reconstituted to 10 mM in water, then to 10 µM in cardiomyocyte maintenance medium and filtered through a 0.22 µm syringe filter. Cells were incubated with each compound and BrdU for 24 h, then fixed and permeabilized as above. Then, to hydrolyze DNA, cells were incubated with 1 M HCl for an hour at room temperature, then neutralized with 0.1 M sodium borate (pH 8.5) for 20 min at room temperature. Next, cells were washed with PBS and immunostaining continued as usual.

Scratch assay. Scratches in 10 mm dishes were done by hand with a 10 µL pipette tip. Scratches in 96-well cell culture polystyrene plates were done using a 200 µL pipette tip and a custom plate lid produced by A.C.N. with a slot designed to guide the pipette tip straight across the well. Media was replaced with media containing NucLight Rapid Red Reagent immediately after scratching and every two days afterward until fixation at specified time points.

Western blotting. Cell lysates were prepared by lysing 50,000 cardiac myocytes with CellLytic (Sigma, St. Louis, MO, #C2978) with 1% protease inhibitor cocktail (P8340, Sigma Aldrich, St. Louis, MO). Gel samples were prepared by mixing cell lysates with LDS sample buffer (Life Technologies, #NP0007) and Sample Reducing Buffer (Life Technologies, #NP00009) and boiled at 95 °C for 5 min. Samples were resolved on Bolt 4–12% gradient Bis–Tris gels (Life Technologies, #NW04120BOX). Protein bands were blotted onto a nylon membrane (Perkin Elmer, Boston MA, NBA085C001EA) with western blotting filter paper (ThermoFisher Scientific, Rockford, IL, #84783). Blots were blocked using 5% nonfat dairy milk (Research Products International Corp, Mt. Prospect, IL, #M17200) in TBST (TBS: Corning, Mannassas, VA, #46-012-CM. Tween20: Sigma, St. Louis, MO, #P9416). Antibody incubations were also performed in 5% NFDM in TBST. Blots were developed using the Immobilon Chemiluminescence Kit (Millipore, #WBKLS0500).

Statistics and quantification. Total YAP was measured in FIJI (ImageJ, NIH, Bethesda, MD) by drawing a polygonal ROI around a cell using a 20 × IncuCyte image stained for B-catenin to mark cell boundaries, and measuring average fluorescence intensity. Nuclear YAP was measured in FIJI by drawing a Bezier ROI around a nucleus using a 20 × IncuCyte image stained for YAP and measuring average fluorescence intensity. Fit of nuclear YAP/total YAP graph in Fig. 1D was determined using the curve fitting toolbox in MatLab (MathWorks, Natick, MA).

Nuclear fold change was determined by thresholding live-cell whole-well 4 × stitches with NucLight Rapid Red Reagent, a live-cell nuclear marker. Thresholding was done using the IncuCyte software (Essen Biosciences, Ann Arbor, MI) and a TopHat Background subtraction using a 20 µM rolling ball. Images were acquired and nuclei counted every hour for specified time points. Nuclei count at the final time point was divided by nuclei count at the first time point and normalized to the average nuclear fold change of cells in control conditions on the same plate.

Statistical significance of Fig. 2D,F were determined by unpaired two-tailed Student's *t* tests performed in Excel. Statistical significance of Figs. 2B and 4C were determined by paired two-tailed Student's *t* tests performed in Excel. Statistical significance of Figs. 3D, 4B,E–G,J were determined by one-way ANOVA with a Dunnett's post-hoc test correcting for multiple testing when applicable performed in GraphPad Prism. Each experiment was performed a minimum of 3 times and the mean of the independent experiments and standard error of the mean (SEM) are displayed.

RNA sequencing. Cell pellets of 100,000 cells were prepared and RNA was extracted using the RNeasy Mini Kit (Qiagen, #74104). Stranded mRNA (polyA-selected) library preparation was completed by the VANTAGE core at Vanderbilt University. Sequencing was done with an Illumina NovaSeq6000 (S4) PE150. Reads were mapped to reference genome using STAR and differential analyses were performed using DESeq2. Differentially expressed genes were determined using the criteria of fold change ≥ 2 and FDR ≤ 0.05. YAP target genes and cardiac myocyte maturity genes were determined from literature and are listed below. Datasets will be uploaded to a public database. N = 3 for each condition, in that each cell treatment and RNA preparation was done three separate times using three separate purchased vials of cells.

Received: 13 April 2021; Accepted: 19 August 2021
Published online: 07 September 2021

References

1. Ponnusamy, M., Li, P. F. & Wang, K. Understanding cardiomyocyte proliferation: An insight into cell cycle activity. *Cell. Mol. Life Sci.* **74**, 1019–1034. https://doi.org/10.1007/s00018-016-2375-y (2017).
2. Porrello, E. R. *et al.* Transient regenerative potential of the neonatal mouse heart. *Science* **331**, 1078–1080. https://doi.org/10.1126/science.1200708 (2011).
3. Laflamme, M. A. & Murry, C. E. Heart regeneration. *Nature* **473**, 326–335. https://doi.org/10.1038/nature10147 (2011).
4. Li, F., Wang, X., Capasso, J. M. & Gerdes, A. M. Rapid transition of cardiac myocytes from hyperplasia to hypertrophy during postnatal development. *J. Mol. Cell. Cardiol.* **28**, 1737–1746. https://doi.org/10.1006/jmcc.1996.0163 (1996).
5. Walsh, S., Ponten, A., Fleischmann, B. K. & Jovinge, S. Cardiomyocyte cell cycle control and growth estimation in vivo—An analysis based on cardiomyocyte nuclei. *Cardiovasc. Res.* **86**, 365–373. https://doi.org/10.1093/cvr/cvq005 (2010).
6. Heallen, T. *et al.* Hippo pathway inhibits Wnt signaling to restrain cardiomyocyte proliferation and heart size. *Science* **332**, 458–461. https://doi.org/10.1126/science.1199010 (2011).
7. Xin, M. *et al.* Hippo pathway effector Yap promotes cardiac regeneration. *Proc. Natl. Acad. Sci. U.S.A.* **110**, 13839–13844. https://doi.org/10.1073/pnas.1313192110 (2013).
8. Dong, J. *et al.* Elucidation of a universal size-control mechanism in Drosophila and mammals. *Cell* **130**, 1120–1133. https://doi.org/10.1016/j.cell.2007.07.019 (2007).
9. He, C. *et al.* The Hippo/YAP pathway interacts with EGFR signaling and HPV oncoproteins to regulate cervical cancer progression. *EMBO Mol. Med.* **7**, 1426–1449. https://doi.org/10.15252/emmm.201404976 (2015).
10. Zhao, B., Li, L., Tumaneng, K., Wang, C. Y. & Guan, K. L. A coordinated phosphorylation by Lats and CK1 regulates YAP stability through SCF(beta-TRCP). *Genes Dev.* **24**, 72–85. https://doi.org/10.1101/gad.1843810 (2010).
11. Gumbiner, B. M. & Kim, N. G. The Hippo-YAP signaling pathway and contact inhibition of growth. *J. Cell Sci.* **127**, 709–717. https://doi.org/10.1242/jcs.140103 (2014).
12. Kim, N. G., Koh, E., Chen, X. & Gumbiner, B. M. E-cadherin mediates contact inhibition of proliferation through Hippo signaling-pathway components. *Proc. Natl. Acad. Sci. U.S.A.* **108**, 11930–11935. https://doi.org/10.1073/pnas.1103345108 (2011).
13. Totaro, A. *et al.* YAP/TAZ link cell mechanics to Notch signalling to control epidermal stem cell fate. *Nat. Commun.* **8**, 15206. https://doi.org/10.1038/ncomms15206 (2017).
14. Zhao, B. *et al.* Inactivation of YAP oncoprotein by the Hippo pathway is involved in cell contact inhibition and tissue growth control. *Genes Dev.* **21**, 2747–2761. https://doi.org/10.1101/gad.1602907 (2007).
15. Schlegelmilch, K. *et al.* Yap1 acts downstream of alpha-catenin to control epidermal proliferation. *Cell* **144**, 782–795. https://doi.org/10.1016/j.cell.2011.02.031 (2011).
16. Varelas, X. The Hippo pathway effectors TAZ and YAP in development, homeostasis and disease. *Development* **141**, 1614–1626. https://doi.org/10.1242/dev.102376 (2014).
17. Kim, J. H., Kushiro, K., Graham, N. A. & Asthagiri, A. R. Tunable interplay between epidermal growth factor and cell-cell contact governs the spatial dynamics of epithelial growth. *Proc. Natl. Acad. Sci. U.S.A.* **106**, 11149–11153. https://doi.org/10.1073/pnas.0812651106 (2009).
18. von Gise, A. *et al.* YAP1, the nuclear target of Hippo signaling, stimulates heart growth through cardiomyocyte proliferation but not hypertrophy. *Proc. Natl. Acad. Sci. U.S.A.* **109**, 2394–2399. https://doi.org/10.1073/pnas.1116136109 (2012).
19. Wang, J., Liu, S., Heallen, T. & Martin, J. F. The Hippo pathway in the heart: Pivotal roles in development, disease, and regeneration. *Nat. Rev. Cardiol.* **15**, 672–684. https://doi.org/10.1038/s41569-018-0063-3 (2018).
20. Park, S. *et al.* Yes-associated protein mediates human embryonic stem cell-derived cardiomyocyte proliferation: Involvement of epidermal growth factor receptor signaling. *J. Cell. Physiol.* **233**, 7016–7025. https://doi.org/10.1002/jcp.26625 (2018).
21. Neininger, A. C., Long, J. H., Baillargeon, S. M. & Burnette, D. T. A simple and flexible high-throughput method for the study of cardiomyocyte proliferation. *Sci. Rep.* **9**, 15917. https://doi.org/10.1038/s41598-019-52467-0 (2019).
22. Uosaki, H. *et al.* Transcriptional landscape of cardiomyocyte maturation. *Cell Rep.* **13**, 1705–1716. https://doi.org/10.1016/j.celrep.2015.10.032 (2015).
23. Sharma, A. *et al.* Stage-specific effects of bioactive lipids on human iPSC cardiac differentiation and cardiomyocyte proliferation. *Sci. Rep.* **8**, 6618. https://doi.org/10.1038/s41598-018-24954-3 (2018).
24. Cory, G. Scratch-wound assay. *Methods Mol. Biol.* **769**, 25–30. https://doi.org/10.1007/978-1-61779-207-6_2 (2011).
25. Hansen, C. G., Ng, Y. L., Lam, W. L., Plouffe, S. W. & Guan, K. L. The Hippo pathway effectors YAP and TAZ promote cell growth by modulating amino acid signaling to mTORC1. *Cell Res.* **25**, 1299–1313. https://doi.org/10.1038/cr.2015.140 (2015).
26. Gerdes, J. *et al.* Cell cycle analysis of a cell proliferation-associated human nuclear antigen defined by the monoclonal antibody Ki-67. *J. Immunol.* **133**, 1710–1715 (1984).
27. Miller, I. *et al.* Ki67 is a graded rather than a binary marker of proliferation versus quiescence. *Cell Rep.* **24**, 1105-1112 e1105. https://doi.org/10.1016/j.celrep.2018.06.110 (2018).

28. D'Uva, G. *et al.* ERBB2 triggers mammalian heart regeneration by promoting cardiomyocyte dedifferentiation and proliferation. *Nat. Cell Biol.* **17**, 627–638. https://doi.org/10.1038/ncb3149 (2015).
29. Wang, W. E. *et al.* Dedifferentiation, proliferation, and redifferentiation of adult mammalian cardiomyocytes after ischemic injury. *Circulation* **136**, 834–848. https://doi.org/10.1161/CIRCULATIONAHA.116.024307 (2017).
30. Venkataramani, V. *et al.* CD31 expression determines redox status and chemoresistance in human angiosarcomas. *Clin. Cancer Res.* **24**, 460–473. https://doi.org/10.1158/1078-0432.CCR-17-1778 (2018).
31. Kim, M. K., Jang, J. W. & Bae, S. C. DNA binding partners of YAP/TAZ. *BMB Rep.* **51**, 126–133. https://doi.org/10.5483/bmbrep.2018.51.3.015 (2018).
32. Lee, D. H. *et al.* LATS-YAP/TAZ controls lineage specification by regulating TGFbeta signaling and Hnf4alpha expression during liver development. *Nat. Commun.* **7**, 11961. https://doi.org/10.1038/ncomms11961 (2016).
33. Fan, F. *et al.* Pharmacological targeting of kinases MST1 and MST2 augments tissue repair and regeneration. *Sci. Transl. Med.* **8**, 352ra108. https://doi.org/10.1126/scitranslmed.aaf2304 (2016).
34. Miller, E. *et al.* Identification of serum-derived sphingosine-1-phosphate as a small molecule regulator of YAP. *Chem. Biol.* **19**, 955–962. https://doi.org/10.1016/j.chembiol.2012.07.005 (2012).
35. Mills, R. J. *et al.* Drug screening in human PSC-cardiac organoids identifies pro-proliferative compounds acting via the mevalonate pathway. *Cell Stem Cell* **24**, 895-907 e896. https://doi.org/10.1016/j.stem.2019.03.009 (2019).
36. Mohamed, T. M. A. *et al.* Regulation of cell cycle to stimulate adult cardiomyocyte proliferation and cardiac regeneration. *Cell* **173**, 104-116 e112. https://doi.org/10.1016/j.cell.2018.02.014 (2018).
37. Liu-Chittenden, Y. *et al.* Genetic and pharmacological disruption of the TEAD-YAP complex suppresses the oncogenic activity of YAP. *Genes Dev.* **26**, 1300–1305. https://doi.org/10.1101/gad.192856.112 (2012).
38. Peter, A. K., Bjerke, M. A. & Leinwand, L. A. Biology of the cardiac myocyte in heart disease. *Mol. Biol. Cell* **27**, 2149–2160. https://doi.org/10.1091/mbc.E16-01-0038 (2016).
39. Triastuti, E. *et al.* Pharmacological inhibition of Hippo pathway, with the novel kinase inhibitor XMU-MP-1, protects the heart against adverse effects during pressure overload. *Br. J. Pharmacol.* **176**, 3956–3971. https://doi.org/10.1111/bph.14795 (2019).
40. Aharonov, A. *et al.* ERBB2 drives YAP activation and EMT-like processes during cardiac regeneration. *Nat. Cell Biol.* **22**, 1346–1356. https://doi.org/10.1038/s41556-020-00588-4 (2020).
41. Ramjee, V. *et al.* Epicardial YAP/TAZ orchestrate an immunosuppressive response following myocardial infarction. *J. Clin. Investig.* **127**, 899–911. https://doi.org/10.1172/JCI88759 (2017).
42. Pfeffer, M. A. & Braunwald, E. Ventricular remodeling after myocardial infarction Experimental observations and clinical implications. *Circulation* **81**, 1161–1172. https://doi.org/10.1161/01.cir.81.4.1161 (1990).
43. Meckert, P. C. *et al.* Endomitosis and polyploidization of myocardial cells in the periphery of human acute myocardial infarction. *Cardiovasc. Res.* **67**, 116–123. https://doi.org/10.1016/j.cardiores.2005.02.017 (2005).
44. Morikawa, Y., Heallen, T., Leach, J., Xiao, Y. & Martin, J. F. Dystrophin-glycoprotein complex sequesters Yap to inhibit cardiomyocyte proliferation. *Nature* **547**, 227–231. https://doi.org/10.1038/nature22979 (2017).

Acknowledgements

We would like to thank the VANTAGE core at Vanderbilt University for RNA Sequencing, and James B. Hayes and Manuel Castro (Vanderbilt University) for careful reading and comments on the manuscript.

Author contributions

A.C.N. and D.T.B. conceived the project and wrote the manuscript. A.C.N. designed, performed, and quantified experiments, and prepared figures. X.D. and Q.L. analyzed RNASeq data.

Funding

This work was supported by the National Institutes of Health (MIRA R35 GM125028 to D.T.B.) and Vanderbilt University School of Medicine Program in Developmental Biology (Training grant T32-HD007502 to A.C.N.).

Competing interests

The authors declare no competing interests.

Additional information

Supplementary Information The online version contains supplementary material available at https://doi.org/10.1038/s41598-021-97133-6.

Correspondence and requests for materials should be addressed to D.T.B.

Reprints and permissions information is available at www.nature.com/reprints.

Publisher's note Springer Nature remains neutral with regard to jurisdictional claims in published maps and institutional affiliations.